Annu. Rev. Phys. Chem. 1992. 43: 153–76

TRANSITION STATE SPECTROSCOPY OF BIMOLECULAR CHEMICAL REACTIONS

Daniel M. Neumark

Department of Chemistry, University of California, Berkeley, California 94720

KEY WORDS: reaction dynamics, potential energy surfaces, resonances, photodissociation, photodetachment

INTRODUCTION

One of the fundamental goals of chemical physics has been to understand the nature of the potential energy surfaces on which chemical reactions occur. Much of this interest focuses on the transition state region: the region of the surface where chemical bonds are broken and reformed. The microscopic forces at play in the transition state region often control the observable properties of a reaction, including the reaction cross-section and the product angular and energy distributions. Indeed, the key issue in chemical reaction dynamics is to deduce the relationship between these asymptotic properties of a reaction and the detailed features of the transition state region, such as (in the case of a direct reaction) the saddle point location, barrier height, and bend potential near the saddle point.

To resolve this issue successfully, one would like to measure the asymptotic properties and experimentally characterize the transition state region for a given reaction. During the last 20 years, most of the experimental emphasis has been on the former aspect; increasingly refined state-to-state scattering experiments have been developed in which final product distributions are measured as a function of well-defined reactant initial conditions (1). These experiments can provide a sensitive, although

0066–426X/92/1101–0153$02.00

indirect, probe of the transition state region. By comparing the experimental results to calculations on proposed potential energy surfaces, one obtains a qualitative understanding of the relationship between the surface and properties of the reaction. This joint approach to reaction dynamics, pioneered by Polanyi (2) in the early 1970s, initially involved comparing product energy and angular distributions with classical trajectory calculations on empirical potential energy surfaces. The tremendous development since then is exemplified in the recent series of experimental and theoretical studies of the $H + H_2$ reaction. Here, measurements of the product state-resolved differential and total cross-sections by Buntin et al (3), Continetti et al (4), Valentini and coworkers (5a,b), and Zare and coworkers (6a,b) agree well (but not perfectly) with exact quantum mechanical scattering calculations performed by Zhang & Miller (7), Truhlar and coworkers (8a,b), Wyatt and coworkers (9a,b), and Launay & LeDourneuf (10) on fully ab initio potential energy surfaces.

This article addresses a conceptually different type of experiment designed to study a reaction while it is in progress, in contrast to state-to-state scattering experiments that look at the products of a reaction long after a reactive collision has occurred. These are generally referred to as transition state spectroscopy experiments, and their goal is to obtain a more direct handle on the nature of the transition state region than is possible from a scattering experiment, by probing the spectroscopy of the reacting species in the vicinity of the transition state. This article reviews the application of transition state spectroscopy to bimolecular chemical reactions. This has proved to be a considerable experimental challenge, because of difficulties involved in studying the short-lived (10^{-12}–10^{-15} s) complex formed in a reactive collision. Thus, for several years following the first experiments of this type of Polanyi and coworkers (11) and Brooks and coworkers (12) in 1980, there was at least as much discussion on whether the results from transition state spectroscopy experiments were real as on what was being learned about reactive potential energy surfaces. However, during the last several years, a variety of frequency and time-domain experiments have been developed that have clearly yielded meaningful and detailed information on the transition state region.

As the status of the field of transition state spectroscopy was extensively reviewed by Brooks (13) in 1988, this article is mainly concerned with more recent experiments. These fall into two categories: full-collision experiments, which probe the complex formed in an actual collision between reactants, and half-collision experiments, which access the transition state region by photoexcitation of a stable precursor. The full-collision studies described below include experiments centered on laser excitation of the complex formed in a collision, experiments designed to

locate quasibound states of the collision complex (reactive resonances), and experiments that probe the complex formed in Penning ionization collisions.

The half-collision transition state spectroscopy experiments include electronic excitation of van der Waals molecules, photodetachment of negative ions, and molecular photodissociation. Because this article focuses on bimolecular reaction dynamics, the discussion of photodissociation studies is restricted to the relatively small number that probe bimolecular potential energy surfaces, i.e. surfaces with a reasonably low energy barrier between distinct reactant and product regions.

FULL-COLLISION STUDIES

Laser Excitation of Colliding Reactants

These experiments, which were first attempted by Hering et al (12) in 1980, aim to alter the course of a reactive (or nonreactive) collision in a detectable way by using laser excitation of the colliding reactants. For example, in Brooks' crossed-beam studies (14a,b) of the reaction

$$K(4^2S) + NaCl \rightarrow KCl + Na(3^2S), \qquad 1.$$

(exothermic by 3.9 kcal/mol), the idea is to excite the transient [KNaCl] complex formed in a collision between reactants with a tunable laser to the excited potential energy surface for the (endothermic) reaction

$$K^*(4^2P) + NaCl \rightarrow KCl + Na^*(3^2P). \qquad 2.$$

The laser wavelength lies between the Na and K $^2P \leftarrow {}^2S$ transitions at 590 and 766 nm, respectively. This excitation is monitored by emission from the Na* produced by reaction on the excited potential energy surface. As the laser is not resonant with any reactant or product transition, Na* emission can only arise when the [KNaCl] complex is excited to a region of the upper surface that leads to Na* formation from Reaction 2. The dependence of this emission signal on excitation wavelength is, in principle, quite sensitive to the form of the transition state regions for Reactions 1 and 2.

In practice, this experiment is extremely challenging, because the steady state concentration of the short-lived [KNaCl] complex is very small, and it must be verified that the observed Na* emission is, indeed, due to excitation of the complex. For example, one must ensure that Na* emission does not arise from the reaction of electronically excited K_2^* (any K_2 in the K beam absorbs between the Na and K transitions), which reacts with NaCl. The most recent results (14b) show that the Na* emission from excitation of the [NaClK] complex is structureless and decreases more or

less monotonically as the excitation wavelength is increased from 600 to 635 nm. In contrast, in the analogous experiment performed on the reaction,

$$K + NaBr \rightarrow KCl + Na, \qquad 3.$$

the Na* emission shows a broad maximum near 605 nm (14b). Yamashita & Morokuma (15, 16) have carried out surface hopping trajectory calculations on ab initio K + NaCl potential energy surfaces and have qualitatively reproduced the Na* emission results for that reaction, but the interpretation of the results for Reaction 3 is unclear at this time. They have applied similar methods in a theoretical study of the Na + HCl reaction (17). The transition state spectroscopy of Reaction 1 has also been modeled by Jiang & Hutchinson (18), who used one-dimensional potentials.

Kleiber and coworkers (19a,b) have used a somewhat different version of laser excitation of collision complexes to initiate the reaction

$$Mg^*(3^1P) + H_2 \rightarrow MgH + H, \qquad 4.$$

which was discussed in the review article by Brooks (13). More recently, Kleiber and coworkers (20a,b) have studied the reaction

$$Na^*(4^2P) + H_2 \rightarrow NaH + H. \qquad 5.$$

The reactions between ground state Mg or Na with H_2 are endothermic, so no reaction occurs in room temperature collisions between ground state reactants. However, the excited state Reactions 4 and 5 are both exothermic. Thus, one can initiate Reaction 5 by exciting the NaH_2 complex formed by a collision between ground state reactants and monitor this by laser-induced fluorescence (LIF) of the NaH product. In this experiment, one not only finds where the complex absorbs, but also how the product rotational distribution varies with excitation energy. These experiments are complementary to the studies by Hering and coworkers (21a,b), who excited the NaH_2 collision complex near the Na D line ($3^2P \leftarrow 3^2S$) and used coherent anti-Stokes Raman spectroscopy (CARS) to look at the H_2 product from inelastic scattering on the excited state surface.

Kleiber and coworkers (20a,b) have found that NaH production is observed whether the complex is excited to the blue or to the red of the Na $4^2P \leftarrow 3^2S$ transition. However, significantly more rotational excitation of the NaH is observed upon excitation to the red. This can be explained

with reference to the Na–H_2 potential energy curves shown in Figure 1, which are based on the pseudopotential calculations by Rossi & Pascale (22). Because the interaction between ground state Na and H_2 is flat at long range, where excitation of the complex is expected, the results are interpreted in terms of accessing two types of excited state potential energy surfaces. Figure 1 shows that the interaction of Na*(4^2P) with H_2 yields an attractive $^2\Pi$ surface for $C_{\infty v}$ symmetry ($^2B_1$, $^2B_2$ in C_{2v} symmetry) and a repulsive $^2\Sigma$ surface ($^2A_1$ in C_{2v}), which also has an entrance channel barrier. Excitation to the attractive surface occurs to the red of the Na transition, whereas excitation to the repulsive surface occurs to the blue. Hence, the results suggest that reaction on the attractive surface, for which side-on C_{2v} approach is the most favorable geometry, leads to considerably more NaH rotational excitation than on the repulsive surface. This picture fits nicely with the bimodal rotational distributions observed in scattering

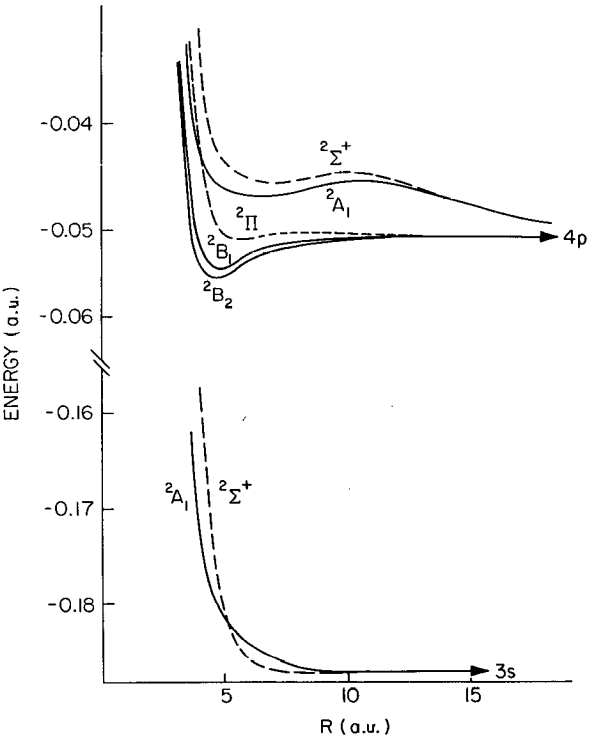

Figure 1 Ground state and excited state potential energy curves for Na + H_2 reactants (from Ref. 20).

studies of the $Na^* + H_2$ and $Mg^* + H_2$ reactions by Bililign & Kleiber (23) and Breckenridge & Umemoto (24), respectively.

The above experiments show that the principle of initiating a reaction via laser excitation of colliding reactants is viable. However, the excitation spectra involve transitions between continuum scattering states supported by two unknown potential energy surfaces. It is, therefore, difficult to extract detailed information on either surface from the results. Clearly, it would be desirable if one or both potential energy surfaces supported some sort of long-lived state of the collision complex, as this might lead to assignable structure in the excitation spectrum. The next section discusses attempts to observe such states in full-collision experiments.

Reactive Resonances in Scattering Experiments

Since the early 1970s (25a–c), quantum mechanical scattering calculations on model potential energy surfaces have predicted sharp structure in the reaction probability (at fixed total angular momentum) as a function of energy. These sharp features, termed reactive resonances, are attributed to the existence of quasibound levels of the collision complex, which live on the order of a few vibrational periods before dissociating. [See the recent review article by Schatz (26).] Resonances are predicted to occur even for direct reactions, such as the $H + H_2$ (25a–c), $F + H_2$ (27), and $Cl + HCl$ (28a,b) reactions, where there is only a barrier and no well in the transition state region. Because the quasibound states responsible for reactive resonances are localized in the transition state region, the spectrum of these resonances should be very sensitive to the details of the reaction potential energy surface in this region. Thus, resonances can play a key role in transition state spectroscopy experiments (29).

Before 1988, the only experimental evidence for reactive resonances were state-resolved differential cross-section measurements by Neumark et al (30) on the $F + H_2$ reaction. However, in 1988, Nieh & Valentini (5b) used CARS to measure absolute reaction cross-sections for H_2 product vibrational and rotational states in the reaction

$$H + \text{para} - H_2(v = 0, j = 0, 2) \rightarrow H_2(v, j) + H. \qquad 6.$$

They found peaks in these cross-sections that roughly corresponded to the calculated positions of reactive resonances for total angular momentum $J = 0$ collisions (8a, 25c, 31). This was a startling result; as Redman & Wyatt (32) first discussed, the energy at which a resonance occurs depends on the orbital angular momentum ℓ of the reactants [$\ell = J$ for $H + H_2(j = 0)$] by approximately $B\ell(\ell + 1)$, where B is a rotational constant appropriate for the collision complex. Thus, in a reactive scattering experiment, where many values of ℓ typically contribute to the reaction,

the contribution of resonances to the total cross-section are expected to average out.

A possible explanation for Valentini's results is that the $H+H_2$ reaction is largely caused by collisions with ℓ near zero and that collisions at higher ℓ simply do not lead to reaction. However, shortly after the experimental results were reported, a series of calculations of the $H+H_2$ reaction cross-section (7–10), which indicated that numerous partial waves contribute to the $H+H_2$ reaction and that resonances should, therefore, average out in state-resolved partial cross-sections. These were exact scattering calculations on accurate, ab initio potential energy surfaces and, therefore, cast doubt on the interpretation of the experimental results. Zare and coworkers (6b) subsequently supported the theoretical results, by experiments in which H_2 rovibrational product distributions were measured with multiphoton ionization and showed no sharp variation with energy. Indeed, Valentini (33) has recently found that the peaks in his experiment disappear at lower fluences than were initially used, which indicates that they are not from variations in the reaction cross-section. Whether they are from laser catalysis, as proposed by Shapiro and coworkers (34a,b), remains to be seen.

In summary, Valentini's $H+H_2$ experiments, and the intense theoretical work that followed them, provide ample evidence for the importance of the concept of resonances in reaction dynamics, but also show just how difficult it is to observe them cleanly in a full-collision experiment. One possible approach is suggested by the recent experiments of Pollard et al (35) in a study of the reaction

$$H_2^+ + He \rightarrow HeH^+ + H, \qquad 7.$$

in which only the forward and back-scattered HeH^+ is detected. Because the back-scattered product is due to collisions at low ℓ, it may be possible to observe variations in this signal as a function of energy because of the extensive resonance structure predicted for this reaction (36a–c). (No structure has yet been resolved.) The subject of reactive resonances appears later in this article, when we discuss half-collision transition state spectroscopy experiments.

Penning Ionization as a Probe of the Collision Complex

In the process of a Penning ionization collision

$$A^* + BC \rightarrow A^+ + BC + e^- \qquad 8.$$

between a highly excited atom A* and a molecule BC, electron ejection can only occur from the [ABC]* complex. The energy spectrum of the ejected electrons depends on the nature of the neutral and ionic potential

energy surfaces that participate in Reaction 8 at nuclear geometries where ionization occurs. Hence, a discussion of recent results in this field is appropriate in a review of transition state spectroscopy.

The connection between Penning ionization and transition state spectroscopy was first advanced by Benz & Morgner (37) in a series of studies on collisions between metastable He (2^3S, 2^1S) with Cl_2, Br_2, and I_2. The resulting Penning ionization electron spectrum (PIES) consists of several broad peaks that clearly correspond to electronic transitions seen in the photoelectron spectra of bare halogen molecules, although the relative intensities are quite different in the two types of spectra. In addition, some intense, broad features at low electron kinetic energy are observed that do not correspond to any peaks seen in the halogen photoelectron spectra. Benz & Morgner attribute these low energy features to a surface crossing from a covalent $He^* \cdot X_2$ surface to a $He^+ \cdot X_2^-$ ion-pair surface before electron ejection. This hypothesis is supported by classical trajectory calculations (including surface hopping) on model potential energy surfaces. However, a detailed interpretation of these experiments is difficult because, once again, several unknown surfaces are involved and only broad features are observed.

In a more recent crossed beam study by Dunlavy et al (38), the PIES for the reaction

$$He^*(2^1S) + N_2 \rightarrow He + N_2^+(X^2\Sigma_g^+, A^2\Pi_u, B^2\Sigma_u^+) + e^- \qquad 9.$$

was obtained at several collision energies between 1.6 and 7 kcal/mol. The energy resolution in this experiment was high enough to resolve vibrational structure associated with each N_2^+ electronic state. The results show that as the collision energy is increased, the intensity of the transitions to the $A^2\Pi_u$ state increases relative to the transitions to the two Σ states. In addition, the vibrational transitions associated with the Π state shift to higher electron energy (a smaller shift is seen for the Σ states). These effects are interpreted in terms of different interaction potentials for a broadside collision of He^* with N_2, which leads to Π state formation, and end-on collisions, which yield Σ states of N_2^+.

HALF-COLLISION STUDIES

A major problem in scattering-based transition state spectroscopy experiments is the extensive averaging over reactant initial conditions. Even if the reactant translational and internal energy is well-controlled, scattering experiments involve averaging over reactant orbital angular momentum (impact parameter) and, in most cases, reactant orientation. This averaging eliminates much, if not all, of the sharp structure that one might see in a

transition state spectroscopy experiment; the $H+H_2$ example discussed above shows, for instance, how angular momentum averaging washes out contributions from reactive resonances to the reaction cross-section.

Averaging over reactant initial conditions is substantially reduced in the half-collision studies described in this section. In these experiments, the idea is to access the transition state region via photoexcitation of a stable precursor, rather than with a scattering event. In most, but not all, of the experiments described below, the angular momentum available to the reactants is highly restricted, compared with a scattering experiment, because the stable precursors are typically formed in a free jet expansion and are rotationally cold. If the photoexcitation process involves either simple photon absorption or ejection of a light particle (i.e. an electron or H atom), then this cold angular momentum distribution is approximately mapped onto the transition region species.

In contrast to scattering experiments, which are sensitive to all reactant orientations that lead to reaction, half-collision experiments typically provide detailed information on the potential energy surface over a restricted geometric range. Although this feature of half-collision experiments is often advantageous, the stable precursor must have good geometric overlap with the transition state region on the upper surface. When this restriction is satisfied, most of the experiments described below yield more readily interpretable results than the full-collision experiments already considered.

Photoexcitation of van der Waals Molecules

An important set of half-collision transition state spectroscopy experiments involve the initiation of bimolecular reactions via photoexcitation of van der Waals molecules. In one set of experiments, one component (typically an atom) of the van der Waals molecule is electronically excited, thereby accessing one or more excited state potential energy surfaces on which reaction occurs. Jouvet & Soep (39) performed the first experiments of this type on the $Hg \cdot Cl_2$ complex. Alternatively, one can photodissociate one member of the van der Waals molecule and study the resulting reaction of one of the photofragments with the other member of the complex. Wittig and coworkers (40a–c) and Zewail and coworkers (41a,b) have pioneered the use of frequency and time-domain methods, respectively, in these studies. Takayanagi & Hanazaki (42) have recently reviewed this overall class of experiments.

In experiments of the first type, which involve electronic excitation of a van der Waals molecule of the form $A \cdot BC$, the idea is to access the excited state potential energy surfaces for the reaction $A^* + BC \rightarrow AB + C$ by exciting this species near the $A^* \leftarrow A$ electronic transition. For a given excitation energy, the AB internal energy distribution can be monitored

by either LIF or, if AB is in an excited electronic state, by dispersing the AB emission. A more fundamental measurement from the point of view of transition state spectroscopy is the action spectrum, in which the product yield is monitored as a function of excitation energy. This maps out the transitions to the upper state surfaces that lead to reaction and is, therefore, a direct probe of these surfaces. These experiments are essentially the half-collision analogue to Kleiber's experiments, which were discussed in the previous section.

During the past few years, Soep, Jouvet, and coworkers have carried out detailed studies of the reactions (43a–c)

$$Hg^*(^3P_1) + H_2 \rightarrow HgH(^2\Sigma^+) + H \qquad 10.$$

and (44a,b)

$$Ca^*(^1D_2, ^1P_1) + HCl \rightarrow CaCl^*(A^2\Pi, B^2\Sigma^+) + H \qquad 11.$$

via excitation of the $Hg \cdot H_2$ and $Ca \cdot HCl$ complexes. In these experiments, one can readily study the effects of orbital alignment, involving the unpaired electrons on the excited atoms, thus providing complementary information to the $Ca^* + HCl$ scattering experiments by Rettner & Zare (45). In the case of Reaction 10, for example, the interaction of $Hg^*(^3P_1)$ with H_2 result in a $^3\Pi$ and $^3\Sigma$ state [more precisely, $\Omega = 0^+$ and 1 states (46)], which are distinct in energy at the geometry of the van der Waals molecule. The action spectrum of the complex and the HgH rotational distribution (both are obtained by LIF on the HgH product) are noticeably different, depending on which upper state surface is accessed. The HgH action spectrum, shown in Figure 2, is of particular interest. This spectrum is broad and unstructured in the region where the Π state of HgH_2 is excited, whereas the Σ action spectrum shows two narrow (6 cm^{-1} wide) peaks that correspond to a vibrational progression in the $Hg–H_2$ stretch. These results imply that reaction on the Π surface is facile, whereas a barrier to reaction exists on the Σ surface that briefly traps the $Hg^* \cdot H_2$ complex. This interpretation is supported by the ab initio calculations of Bernier & Millie (47).

In the $Ca \cdot HCl$ experiment, action spectra obtained by monitoring CaCl* emission showed bands to the red and blue of both the $Ca\ ^1P_1 \leftarrow {}^1S_0$ and $^1D_2 \leftarrow {}^1S_0$ transitions. The most interesting of these is the Σ band to the red of the $^1P_1 \leftarrow {}^1S_0$ transition (44a), which shows an extended progression in hindered rotational levels of the upper state. A fit of the peak positions and intensity distribution of this band indicates that it is caused by a transition from a linear Ca–H–Cl ground state to a T-shaped excited state. The peak widths in this band show that the upper state lives for several vibrational periods before dissociating to products. The

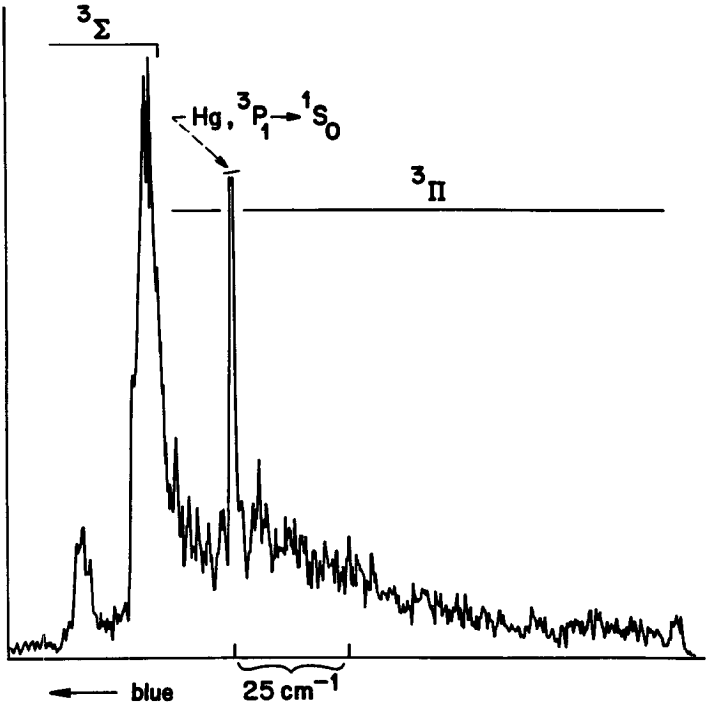

Figure 2 HgH action spectrum obtained via excitation of the $Hg \cdot H_2$ van der Waals molecule (from Ref. 43).

presence of sharp peaks in this progression shows that excitation of the complex does not directly access the dissociative $Ca^+ \cdot HCl^-$ charge transfer state, which correlates to the reaction products.

In an example of the second type of van der Waals excitation experiment, the reaction

$$H + CO_2 \rightarrow OH + CO \qquad 12.$$

is initiated by photodissociating the HBr in the complex $HBr \cdot CO_2$. This yields translationally hot H atoms, which collide with the CO_2 over a restricted angular range determined by the geometry and zero point motion of the van der Waals molecule. In the experiments of Wittig and coworkers (40a–c), the energy distribution of the resulting OH product is measured and compared with the corresponding distribution obtained in hot-atom, full-collision experiments on the $H + CO_2$ reaction, which sample all reactant orientations. In general, the OH rotational distributions are narrower in the half-collision experiment for the same photolysis wavelength. Similar

results are seen in photolysis of the $HI \cdot CO_2$ (48a,b) and $H_2S \cdot CO_2$ (49) complexes. Although this effect was initially attributed to the narrower range of reactant orientations in the half-collision experiment, it is now believed to result primarily from the lowered effective translation energy of the H atom because of its interaction with the departing Br atom (50). The effect of the Br atom on the $H+CO_2$ reaction dynamics has been treated theoretically by Shin et al (51) and Kudla & Schatz (52).

Additional experiments of this type have yielded an explicit correlation between reactant orientation and reactivity. Infrared spectra of the van der Waals molecules by Sharpe et al (53) show that $HCl \cdot CO_2$ has a linear equilibrium geometry with the H atom between the Cl and an O atom, whereas $HBr \cdot CO_2$ has a T-shaped $Br–CO_2$ equilibrium geometry with the H–Br bond nearly parallel to the CO_2. Shin et al (54) found the OH yield from photodissociation of $HBr \cdot CO_2$ to be considerably higher than from photodissociation of $HCl \cdot CO_2$. This is a surprising result, because based on the equilibrium geometry of $HBr \cdot CO_2$, one would expect the H atom to miss the CO_2 entirely. However, the large zero-point angular motion of the H atom in $HBr \cdot CO_2$ enables broadside attack by the H atom at one of the O atoms. The experiment thus indicates that this broadside approach is more likely to lead to reaction than the collinear approach of the H atom that occurs when $HCl \cdot CO_2$ is photodissociated.

Other reactions studied by this method include the $H+N_2O$ reaction, initiated by photolysis of $HI \cdot N_2O$ (54, 55) or $HBr \cdot N_2O$ (56); the D + OCS reaction, initiated by photolysis of DBr · OCS (57); and the $O(^1D)+N_2O$ reaction, initiated by photolysis of $(N_2O)_2$ (58a,b).

Whereas the above experiments have taken advantage of the restricted reactant orientation that occurs in the photolysis of van der Waals precursors to a reaction, Zewail, Bernstein, and coworkers (41a,b) have exploited the fact that the photolysis of such a precursor with a short laser pulse can provide a zero-of-time for a bimolecular reaction. In these experiments, a pair of picosecond or femtosecond pulses is used to initiate the reaction and then detect product formation as a function of the delay time between the pulses, thereby providing a real-time clock of the reaction rate.

The first measurements of this type were performed on Reaction 12 by Scherer and coworkers (41a,b), who used picosecond pulses to photolyze $HI \cdot CO_2$ and detect the OH product. Production of OH clearly occurs on a several picosecond time scale, and a more detailed fitting of the data yields two time constants: τ_1, for formation of the HOCO intermediate (possibly including the time required for isomerization from the *cis* to *trans* form); and τ_2, for dissociation of the HOCO to OH + CO. As the photolysis wavelength is decreased from 264 to 231 nm, τ_1 remains con-

stant around 1 ps, whereas τ_2 decreases from 5 to 0.5 ps. The increased dissociation rate with energy is in qualitative agreement with RRKM calculations. These time-resolved measurements provide an important set of parameters that must be reproduced by any model potential energy surface proposed for this reaction (59a–c).

More recently, Gruebele et al (60) have studied the reaction

$$Br + I_2 \rightarrow IBr + I \qquad 13.$$

by using femtosecond lasers to photolyze the van der Waals molecule $HBr \cdot I_2$ and monitor the production of IBr. This is a kinematically cleaner experiment than the $HX \cdot CO_2$ studies, because a fast light atom, rather than a slow heavy atom, is ejected away from the complex by photolysis. This leads to less interaction of the reaction complex with the ejected atom and means that less angular momentum is transferred to the complex. In any case, the IBr rise time is about 50 ps, considerably slower than the product rise time in the $HI \cdot CO_2$ experiment. The slow rise time is largely caused by the low translational energy of the Br atom ($\sim 200\ cm^{-1}$). This result agrees with classical trajectory calculations on a model potential energy surface with a 15 kcal/mol well relative to the $Br + I_2$ reactants and a 3.5 kcal/mol exit barrier.

Strictly speaking, neither the frequency nor time-domain van der Waals photodissociation studies are transition state spectroscopy experiments, because they probe the asymptotic OH or IBr products, rather than the short-lived HOCO or BrI_2 intermediate. However, they represent new and conceptually appealing techniques that provide information on the transition state region (most favorable reactant orientation, lifetime of the complex), which is often difficult to extract from conventional scattering experiments. In addition, in contrast to the experiments of Soep and coworkers, these experiments access the ground state potential energy surface for a reaction and, therefore, have a stronger link to scattering and kinetics experiments.

Negative Ion Photodetachment Experiments

Another half-collision method to study bimolecular transition states has been developed in our laboratory during the past few years (61). These experiments are conceptually similar to those of Soep and coworkers. However, we use photodetachment of stable negative ions, rather than electronic excitation of van der Waals molecules, to access the transition state. For example, photodetachment of the IHI^- anion forms an unstable IHI complex, which lies in the transition state region for the I+HI reaction. The IHI^- photoelectron spectrum (62) and the higher resolution (0.4 meV) threshold photodetachment (63) spectrum, both of which are

shown in Figure 3, reveal well-resolved vibrational structure attributed to the IHI complex that provides a detailed probe of the I+HI transition state region. Depending on the anion molecular orbital from which the electron is ejected, we can access either the ground or excited state potential energy surfaces for the neutral reaction (61); transitions to the various surfaces appear at different energies in the photodetachment spectrum.

As in Soep's experiments, we are able to restrict the angular momentum available to the neutral reaction. The anions are formed in a pulsed free jet expansion and are rotationally cold (10–50 K), and the ejection of an electron transfers very little angular momentum to the IHI complex. In addition, an anion such as IHI^- is more tightly bound than a typical van der Waals molecule, which means that the range of reactant orientations is even more restricted than in the van der Waals excitation experiments. This control over reaction angular momentum and reactant orientation allows us to observe structure in the photodetachment spectrum that would be averaged out in a scattering experiment.

Most of the photodetachment experiments have involved photodetachment of hydrogen-bonded AHB^- anions to study the transition state region of the heavy+light-heavy reaction $A+HB \rightarrow HA+B$. Specific examples include the following reactions: the symmetric hydrogen exchange reactions

$$X+HX \rightarrow HX+X(X = Cl, Br, I) \qquad 14.$$

studied by photodetachment of $ClHCl^-$ (64a), $BrHBr^-$ (64b), and IHI^-

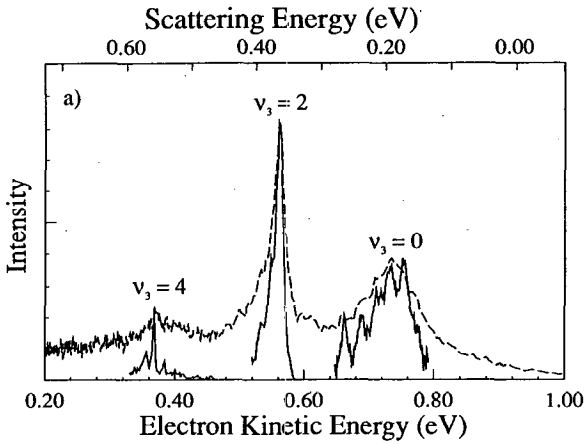

Figure 3 Threshold photodetachment spectrum of IHI^- (——) superimposed on lower resolution photoelectron spectrum (– – –) (from Ref. 75). Peak labeling refers to antisymmetric stretch quantum number (v_3) of IHI complex.

(62, 63), reactions involving hydrogen exchange between two different halogen atoms

$$X + HI \rightarrow HX + I (X = F, Cl, Br)$$

$$F + HBr \rightarrow HF + Br \qquad 15.$$

studied by photodetachment of FHI^-, $ClHI^-$, $BrHI^-$ (65), and $FHBr^-$ (61), and other hydrogen abstraction reactions of fluorine

$$F + CH_3OH \rightarrow HF + CH_3O$$

$$F + OH \rightarrow HF + O(^3P), O(^1D)$$

$$F + H_2 \rightarrow HF + H \qquad 16.$$

studied by photodetachment of CH_3OHF^- (66), OHF^- (66), and H_2F^- (67a–c). All but the $F + H_2$ reaction are heavy + light-heavy reactions.

All of these reactions are believed to be direct; their potential energy surfaces have barriers, but no wells, in the transition state region. Nonetheless, the photoelectron spectra of the above anions show vibrational progressions characteristic of the neutral transition state region. In the heavy + light-heavy reactions, these progressions are caused by the rapid vibrational motion of the H atom between the heavy end atoms (the ν_3 antisymmetric stretch in XHX complexes); several of these vibrations occur before the neutral AHB complex dissociates. The peaks in Figure 3 are labeled by the ν_3 quantum number in the IHI complex. Although the peak positions allow one to map out these vibrational energy levels, the peak widths are an indication of the dissociation dynamics of the complex.

Figure 3 illustrates that the higher resolution threshold photodetachment spectrum of IHI^- (63) shows two types of additional structure. The $\nu_3 = 2$ and 4 peaks are actually composed of progressions in the low-frequency symmetric stretch mode of IHI, which are due to quasibound states of the complex, some of which live at least 200 fs before dissociating. These quasibound states are the very ones that lead to resonances in the I + HI reaction, and the resolution of these features represents the first definitive observation of reactive resonances, which verifies the predictions of sharp resonances in heavy + light-heavy reactions by Manz and coworkers (28a, 68) and Pollak (28b). In addition, the $\nu_3 = 0$ peak is composed of a progression in hindered rotor levels of the IHI complex, because of rotational motion of the H atom around one of the I atoms that occurs on the same time scale as dissociation of the complex.

To relate the photodetachment spectra to reactive potential energy surfaces, it is useful to compare the experimental spectra with quantum mechanical simulations on model surfaces. We have simulated the IHI^-

(62) and $BrHBr^-$ (64a,b) spectra on collinear potential energy surfaces by using time-independent methods in which the Franck-Condon overlap between the anion and neutral scattering wavefunctions is calculated as a function of energy. The comparison between experimental and simulated $BrHBr^-$ spectra was used to develop an improved potential energy surface for the Br + HBr reaction. The $BrHI^-$ spectrum was simulated by using time-dependent wavepacket propagation methods, which yield a clear physical picture of the dissociation dynamics of the BrHI complex (65). The OHF^- photoelectron spectrum was also simulated with time-dependent methods (66), thus resulting in an improved F + HO triplet surface.

More sophisticated simulations on three-dimensional potential energy surfaces have been carried out by Schatz (69), Bowman and coworkers (70a,b), and Zhang & Miller (67b, 71). The simulations of the $ClHCl^-$, IHI^-, and IDI^- spectra by Schatz and of the H_2F^- spectrum by Zhang & Miller were exact, in that they calculate the Franck-Condon overlap between the anion ground state and the three-dimensional scattering wavefunction on the neutral model potential energy surface. The calculations were restricted to total angular momentum $J = 0$, but as the anions in the experiment are rotationally cold, it is reasonable to compare the simulations with the experimental results. Schatz's simulations show both the resonance and hindered rotor structure seen in the high resolution IHI^- threshold photodetachment spectrum, whereas a comparison between Zhang & Miller's H_2F^- and D_2F^- simulations with the experimental photoelectron spectra led to an identification of some experimental peaks as reactive resonances.

In other theoretical work on these systems, Yamashita & Morokuma (72) showed that the $ClHCl^-$ spectrum may contain transitions to excited Cl + HCl surfaces. Taylor and coworkers (73a,b) have simulated the $ClHCl^-$ and FH_2^- spectra by using classical mechanics and analyzed the structure in the spectrum in terms of periodic orbits. Kubach et al (74) have developed a three-dimensional adiabatic picture for the I + HI reaction, which we have adopted in an analysis of the IHI^- spectrum (75). Grayce & Skodje (76) have proposed an alternative three-dimensional adiabatic scheme, which holds promise for accurate, but approximate, simulations of the IHI^- spectrum.

Although transition state spectroscopy using negative ion photodetachment is a powerful technique, it does require good geometric overlap between the anion and neutral transition state region. In addition, to extract detailed information on the neutral potential energy surface, the anion must be well characterized. Geometries and vibrational frequencies have been experimentally determined for only a handful of negative ions, so one must rely on ab initio calculations for this information.

Photodissociation of Stable Molecules

No discussion of half-collision transition state spectroscopy experiments is complete without considering what can be learned about transition states from the photodissociation of stable molecules. The variety of excited electronic states that can be studied in photodissociation is considerable (77), and a complete discussion of the recent experimental and theoretical investigations in this area would fill an entire review article. In the spirit of this article, the discussion of photodissociation is restricted to those experiments that probe excited states with bimolecular potential energy surfaces that have a relatively low energy saddle point between reactant and product valleys. If the ground state and saddle point geometries are similar, one can perform transition state spectroscopy on an excited state potential energy surface for a bimolecular reaction. As examples, frequency-domain photodissociation studies of H_2O, H_2S, and CH_3SH and time-domain studies of HgI_2 are discussed below.

Although the most common frequency-domain experiments are those in which the photofragment asymptotic final state distributions are measured, two other types of measurements are better examples of transition state spectroscopy experiments. The first and most straightforward is photoabsorption, which, assuming the ground state is well characterized, maps out the excited potential energy surface in the Franck-Condon accessible region. Such a measurement is exactly analogous to the anion photoelectron spectroscopy experiments described in the previous section. In addition, Kinsey and coworkers (78a,b) showed that, subsequent to excitation, one could observe vibrationally resolved emission from the dissociating excited state, thereby learning how the geometry and vibrational modes of the molecule evolve as it dissociates. This experiment is essentially resonance Raman spectroscopy with a dissociative upper state; loosely speaking, it is a half-collision version of Polanyi's original state spectroscopy experiment (11). Kinsey's method unfortunately requires high concentrations of the species of interest and, so far, has not been used in experiments in which van der Waals molecules or negative ions are the transition state precursor.

A prime example of an electronic transition from a stable molecule in which the upper state is similar to that of a direct bimolecular reaction is the $\tilde{A}(^1B_1) \leftarrow \tilde{X}(^1A_1)$ band in H_2O. Ab initio calculations by Staemmler & Palma (79) on the $\tilde{A}$ state yield a surface with a 2 eV barrier along the minimum energy path from $H+OH\ \tilde{X}(^2\Pi)$ reactants to (identical) products. The $\tilde{A} \leftarrow \tilde{X}$ absorption band, centered at $\lambda = 165$ nm, shows diffuse structure with a characteristic spacing of about 1750 cm^{-1} (80). Although this structure was initially believed to be a bend progression, the

spectrum was recently analyzed by Engel et al (81) and Imre and coworkers (82a,b), who used time-independent and time-dependent methods, respectively. These authors demonstrated that the structure arises from symmetric stretch motion of the dissociating H_2O molecule. The mechanism for this is identical to that proposed by Pack (83), Heller (84), and Kulander & Light (85) in their model calculations on photodissociation of symmetric triatomic molecules. Excitation from the ground state accesses the ridge between the reactant and product valleys, but at a smaller OH distance and, hence, at a higher energy than the saddle point geometry. This ridge is parallel to the symmetric stretch coordinate. On a bound potential energy surface, such a displacement would lead to a symmetric stretch progression in the absorption spectrum. On the $\tilde{A}$ state surface, which is repulsive along the antisymmetric stretch coordinate, the progression is still apparent, but the peaks are broadened significantly because of the prompt dissociation of the H_2O molecule.

Resonance Raman spectra of the $\tilde{A} \leftarrow \tilde{X}$ transition in H_2O have been performed by Sension et al (86) at several wavelengths within the band. Zhang & Imre (82b) have simulated these spectra by using time-dependent wavepacket analysis. The emission spectra show extended progressions in the OH stretches, which, for the H_2O ground state, are better described in a local mode basis than a normal mode basis. The vibrational levels of H_2O populated by emission from the dissociating molecule have significant symmetric stretch excitation, which indicates that this is the motion that dominates the early dissociation dynamics of the $\tilde{A}$ state. No progressions in the bending modes are observed, which indicates little bending motion as dissociation occurs. This is consistent with the small amount of rotational excitation in the OH fragment seen in product state-resolved studies of $\tilde{A}$ state dissociation by Andresen and coworkers (87a,b). Zhang et al (88) have recently looked at $\tilde{C}(^1B_1) \rightarrow \tilde{A}$ emission in H_2O to gain further insight into the dissociation dynamics of the $\tilde{A}$ state.

The first absorption band of H_2S around $\lambda = 195$ nm (89) also shows diffuse structure attributed to rapid dissociation, and resonance Raman spectra of this band taken by Kleinermanns et al (90), Person et al (91), and Brudzynski et al (92) are dominated by SH stretching progressions. At first glance, these results suggest a similar mechanism to that of the H_2O $\tilde{A}$ state photodissociation. However, ab initio calculations indicate H_2S has two closely lying excited states in the vicinity of the first absorption band (93a–c): a repulsive $^1B_1$ state and a bound $^1A_2$ state. (Both states are of A″ symmetry for C_s geometries.) The resonance Raman spectrum of Brudzynski et al (92) varies as the wavelength of the excitation laser is scanned across the band; no such variation was seen in the analogous H_2O experiment (86). They attributed this effect to vibronic coupling between

the two excited states. Dixon et al (94) and Schinke et al (95) have analyzed the structure in the absorption band and concluded that it also arises from the interaction of the two excited states; the structure is from symmetric stretch motion in the $^1A_2$ state, which is predissociated by the repulsive $^1B_1$ state. The picture of the dissociation dynamics in H_2S is, therefore, substantially more complicated than the isolated $\tilde{A}$ state dissociation in H_2O.

A similar situation arises in the case of CH_3SH photodissociation. The $^1A''$ excited state surface correlates adiabatically from $H+CH_3S$ reactants to CH_3+SH products. Molecular beam photofragmentation studies by Nourbakhsh et al (96) and Keller et al (97) show that photodissociation at 193 nm yields both products, with S–H bond fission dominating. However, Keller et al's emission spectroscopy results only show activity in the C–S stretch and none in the S–H stretch. This suggests that the initial excitation is to the $2^2A''$ state, which is bound along the S–H stretch (98), and that this state is coupled to the bimolecular $1^1A'$ surface via a breakdown of the Born-Oppenheimer approximation.

Zewail and coworkers have pioneered the application of femtosecond pulse techniques to provide a real-time probe of photodissociation. This method was first used to look at diatomic and quasidiatomic photodissociation [NaI (99) and ICN (100), respectively], but more recently has been applied to the photodissociation of HgI_2 at 310 nm (101a,b). This accesses two excited state surfaces, which are bimolecular potential energy surfaces for the $I(^2P_{3/2})+HgI(X^2\Sigma)$ and $I^*(^2P_{1/2})+HgI(X^2\Sigma)$ exchange reactions. In these experiments, HgI_2 is excited with a 50–90 fs pulse at $\lambda_1 = 310$ nm. The resulting dissociation dynamics are monitored via the LIF signal that results from a second short pulse at wavelength λ_2, whose delay relative to the first pulse can be adjusted. The LIF signal is dispersed, and the emission intensity at various wavelengths is measured as a function of the delay time.

Most of the experiments were done at $\lambda_2 = 390$ nm, where the probe laser is resonant with the HgI $B^2\Sigma \leftarrow X^2\Sigma$ transition. These experiments yield emission signals that show transients at short times (0–200 fs); at longer times, they show oscillations with periods varying from 200–1000 fs, depending on the wavelength of the emission. Wavepacket simulations by Grubele et al (102) on model potential energy surfaces yield considerable insight into the origin of these features (see Figure 4). This simulation shows that the initially prepared wavepacket moves along the symmetric stretch coordinate and spreads out over the I+Hg+I three-body dissociation plateau (the HgI bond strength is only 2800 cm^{-1}). Only after this spreading out occurs does the wavepacket develop significant amplitude in the HgI+I(I*) valleys. The calculations suggest that the short-time

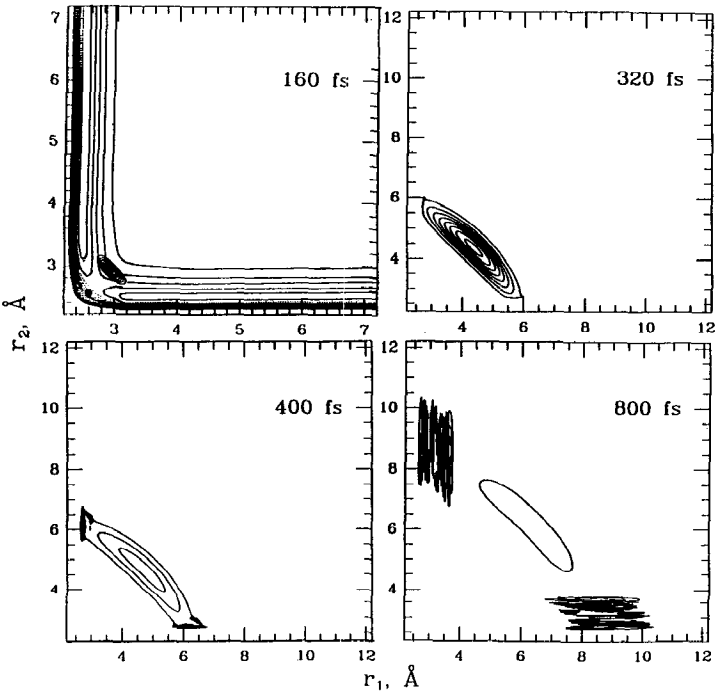

Figure 4 Wavepacket simulation for HgI_2 complex following excitation to model potential energy surface for $I^*(^2P_{1/2}) + HgI \rightarrow HgI + I^*$. Note significant spreading of initial wavepacket into I + Hg + I plateau at early times ($\leq$400 fs) (from Ref. 102).

transients are from the initial large amplitude symmetric stretch motion, whereas the oscillations at longer times are caused by vibrational motion of the HgI in the valleys. Transients were also seen in experiments performed at a probe laser wavelength $\lambda_2 = 620$ nm. This wavelength is not resonant with any HgI transition, and the transients presumably result from even earlier time dynamics of the dissociating IHgI complex.

To summarize, photodissociation of stable molecules can be a powerful probe of excited state surfaces for bimolecular reactions. The ease of obtaining high concentrations of stable molecules enables a greater variety of experiments to be performed, compared with other half-collision experiments in which the transition state precursor is more difficult to prepare. On the other hand, photodissociation experiments often access multiple interacting electronic states, and these interactions must be sorted out and understood to explain the experimental observations.

SUMMARY

This article has covered recent developments in the field of transition state spectroscopy of bimolecular chemical reactions. The various full- and half-collision experiments designed to probe the transition state have been discussed, along with the theoretical treatments developed to analyze these experiments. It is fair to say that, over the last five years, most of the successful transition state spectroscopy studies have been half-collision experiments. This trend is likely to continue in the short term, as the various techniques described here are applied to more complex chemical reactions. One also expects various combinations of half-collision methods to arise, in which, for example, real-time or resonance Raman experiments are performed on reactions initiated by electronic excitation of a van der Waals molecule or by negative ion photodetachment. Finally, the development of new full-collision transition state spectroscopy experiments over the next several years is likely and holds considerable promise for further qualitative breakthroughs in this area.

ACKNOWLEDGMENTS

The results reported from our laboratory are due to the hard work of several current and former members of my research group: Stephen Bradforth, Don Arnold, Dr. Ricardo Metz, Dr. Alexandra Weaver, Dr. Theofanis Kitsopoulos, and Prof. Irene Waller. Support from the Air Force Office of Scientific Research under Grant No. AFOSR-91-0084 is gratefully acknowledged.

Literature Cited

1. Levine, R. D., Bernstein, R. B. 1987. *Molecular Reaction Dynamics and Chemical Reactivity*. New York: Oxford Univ. Press. 535 pp.
2. Polanyi, J. C. 1972. *Acc. Chem. Res.* 5: 161–68
3. Buntin, S. A., Giese, C. F., Gentry, W. R. 1987. *J. Chem. Phys.* 87: 1443–45
4. Continetti, R. E., Balko, B. A., Lee, Y. T. 1990. *J. Chem. Phys.* 93: 5719–40
5a. Gerrity, D. P., Valentini, J. J. 1983. *J. Chem. Phys.* 79: 5202–3
5b. Nieh, J.-C., Valentini, J. J. 1988. *Phys. Rev. Lett.* 60: 519–22; Nieh, J.-C., Valentini, J. J. 1990. *J. Chem. Phys.* 92: 1083–97
6a. Marinero, E. E., Rettner, C. T., Zare, R. N. 1984. *J. Chem. Phys.* 80: 4142–56
6b. Kliner, D. A. V., Adelman, D. E., Zare, R. N. 1991. *J. Chem. Phys.* 94: 1069–80
7. Zhang, J. Z. H., Miller, W. H. 1988. *Chem. Phys. Lett.* 153: 465–70; Zhang, J. Z. H., Miller, W. H. 1989. *J. Chem. Phys.* 91: 1528–47; Zhang, J. Z. H., Miller, W. H. 1989. *Chem. Phys. Lett.* 159: 130–33; Miller, W. H. 1990. *Annu. Rev. Phys. Chem.* 41: 245–81
8a. Mladenovic, M., Zhao, M., Truhlar, D. G., Schwenke, D. W., Sun, Y., Kouri, D. J. 1988. *Chem. Phys. Lett.* 146: 358–63; Mladenovic, M., Zhao, M., Truhlar, D. G., Schwenke, D. W., Sun, Y., Kouri, D. J. 1988. *J. Phys. Chem.* 92: 7035–38
8b. Zhao, M., Truhlar, D. G., Schwenke, D. W., Kouri, D. J. 1990. *J. Phys. Chem.* 94: 7074–90

9a. Manolopoulos, D. E., Wyatt, R. E. 1989. *Chem. Phys. Lett.* 159: 123–29
9b. D'Mello, M. D., Manolopoulos, D. E., Wyatt, R. E. 1991. *J. Chem. Phys.* 94: 5985–93
10. Launay, J. M., LeDourneuf, M. 1989. *Chem. Phys. Lett.* 163: 178–88
11. Arrowsmith, P., Bartoszek, F. E., Bly, S. H. P., Carrington, T., Charters, P. E., Polanyi, J. C. 1980. *J. Chem. Phys.* 73: 5895–97
12. Hering, P., Brooks, P. R., Curl, R. F., Judson, R. S., Lowe, R. S. 1980. *Phys. Rev. Lett.* 44: 687–90
13. Brooks, P. R. 1988. *Chem. Rev.* 88: 407–28
14a. Maguire, T. C., Brooks, P. R., Curl, R. F., Spence, J. H., Ulvick, S. J. 1986. *J. Chem. Phys.* 85: 844–55
14b. Barnes, M. D., Brooks, P. R., Curl, R. F., Harland, P. W. 1991. *J. Chem. Phys.* 94: 5245–47
15. Yamashita, K., Morokuma, K. 1989. *J. Chem. Phys.* 91: 7477–89
16. Yamashita, K., Morokuma, K. 1988. *J. Phys. Chem.* 92: 3109–16
17. Yamashita, K., Morokuma, K. 1990. *Chem. Phys. Lett.* 169: 263–68
18. Jiang, J., Hutchinson, J. S. 1987. *J. Chem. Phys.* 87: 6973–82
19a. Kleiber, P. D., Lyrra, A. M., Sando, K. M., Heneghan, S. P., Stwalley, W. C. 1985. *Phys. Rev. Lett.* 54: 2003–6
19b. Kleiber, P. D., Lyrra, A. M., Sando, K. M., Zafiropoulos, V., Stwalley, W. C. 1986. *J. Chem. Phys.* 85: 5493–5540
20a. Bililign, S., Kleiber, P. D. 1990. *Phys. Rev. A* 42: 6938–41
20b. Bililign, S., Kleiber, P. D., Kearney, W. R., Sando, K. M. 1992. *J. Chem. Phys.* 96: 218–29
21a. Hering, P., Cunha, S. L., Kompa, K. L. 1987. *J. Phys. Chem.* 91: 5459–62
21b. de Vivie-Riedle, R., Hering, P., Kompa, K. L. 1990. *Z. Phys. D* 17: 299–308
22. Rossi, F., Pascale, J. 1985. *Phys. Rev. A* 32: 2657–69
23. Bililign, S., Kleiber, P. D. 1992. *J. Chem. Phys.* 96: 213–17
24. Breckenridge, W. H., Umemoto, H. 1984. *J. Chem. Phys.* 80: 4168–76
25a. Truhlar, D. G., Kuppermann, A. 1970. *J. Chem. Phys.* 52: 3841–43
25b. Levine, R. D., Wu, S.-F. 1971. *Chem. Phys. Lett.* 11: 557–61
25c. Schatz, G. C., Kuppermann, A. 1975. *Phys. Rev. Lett.* 35: 1266–69
26. Schatz, G. C. 1988. *Annu. Rev. Phys. Chem.* 39: 317–40
27. Schatz, G. C., Bowman, J. M., Kuppermann, A. 1975. *J. Chem. Phys.* 63: 674–84
28a. Bondi, D. K., Connor, J. N. L., Manz, J., Romelt, J. 1983. *Mol. Phys.* 50: 467–88
28b. Pollak, E. 1983. *J. Chem. Phys.* 78: 1228–36
29. Kuppermann, A. 1981. In *Potential Energy Surfaces and Dynamics Calculations*, ed. D. G. Truhlar, pp. 375–420. New York: Plenum. 866 pp.
30. Neumark, D. M., Wodtke, A. M., Robinson, G. N., Hayden, C. C., Lee, Y. T. 1985. *J. Chem. Phys.* 82: 3045–66
31. Webster, F., Light, J. C. 1986. *J. Chem. Phys.* 85: 4744–45
32. Redmon, M. J., Wyatt, R. E. 1979. *Chem. Phys. Lett.* 63: 209–12
33. Valentini, J. J. 1991. *Faraday Discuss. Chem. Soc.* 91: 392–93
34a. Seideman, T., Shapiro, M. 1988. *J. Chem. Phys.* 88: 5525–35
34b. Seideman, T., Krause, J. L., Shapiro, M. 1991. *Faraday Discuss. Chem. Soc.* 91: 271–88
35. Pollard, J. E., Syage, J. A., Johnson, L. K., Cohen, R. B. 1991. *J. Chem. Phys.* 94: 8615–17
36a. Zhang, J. Z. H., Yeager, D. L., Miller, W. H. 1990. *Chem. Phys. Lett.* 173: 489–95
36b. Kress, J. D., Walker, R. B., Hayes, E. F. 1990. *J. Chem. Phys.* 93: 8085–97
36c. Lepetit, B., Launay, J. M. 1991. *J. Chem. Phys.* 95: 5159–68
37. Benz, A., Morgner, H. 1986. *Mol. Phys.* 57: 319–36; Benz, A., Morgner, H. 1986. *Mol. Phys.* 58: 223–55
38. Dunlavy, D. C., Martin, D. W., Siska, P. E. 1990. *J. Chem. Phys.* 93: 5347–48
39. Jouvet, C., Soep, B. 1983. *Chem. Phys. Lett.* 96: 426–28
40a. Buelow, S., Radhakrishnan, G., Catanzarite, J., Wittig, C. 1985. *J. Chem. Phys.* 83: 444–45
40b. Radhakrishnan, G., Buelow, S., Wittig, C. 1986. *J. Chem. Phys.* 84: 727–38
40c. Buelow, S., Noble, M., Radhakrishnan, G., Reisler, H., Wittig, C., Hancock, G. 1986. *J. Phys. Chem.* 90: 1015–27
41a. Scherer, N. F., Khundkar, L. R., Bernstein, R. B., Zewail, A. H. 1987. *J. Chem. Phys.* 87: 1451–53
41b. Scherer, N. F., Sipes, C., Bernstein, R. B., Zewail, A. H. 1990. *J. Chem. Phys.* 92: 5239–59
42. Takayanagi, M., Hanazaki, I. 1991. *Chem. Rev.* 91: 1193–1212
43a. Breckenridge, W. H., Jouvet, C., Soep, B. 1986. *J. Chem. Phys.* 84: 1443–50
43b. Jouvet, C., Boiveneau, M., Duval, M.

C., Soep, B. 1987. *J. Phys. Chem.* 91: 5416–22
43c. Jouvet, C., Duval, M. C., Soep, B., Breckenridge, W. H., Whitham, C., Visticot, J. P. 1989. *J. Chem. Soc. Faraday Trans. 2* 85: 1133–40
44a. Visticot, J. P., Soep, B., Whitham, C. J. 1988. *J. Phys. Chem.* 92: 4574–76
44b. Soep, B., Whitham, C. J., Keller, A., Visticot, J. P. 1991. *Faraday Discuss. Chem. Soc.* 91: 191–206
45. Rettner, C. T., Zare, R. N. 1981. *J. Chem. Phys.* 75: 3636–37; Rettner, C. T., Zare, R. N. 1982. *J. Chem. Phys.* 77: 2416–29
46. Duval, M.-C., Soep, B., Breckenridge, W. H. 1991. *J. Phys. Chem.* 95: 7145–53
47. Bernier, A., Millie, P. 1988. *J. Chem. Phys.* 4843–54
48a. Chen, Y., Hoffman, G., Oh, D., Wittig, C. 1989. *Chem. Phys. Lett.* 159: 426–34
48b. Hoffman, G., Oh, D., Chen, Y., Engel, Y. M., Wittig, C. 1990. *Is. J. Chem.* 30: 115–29
49. Rice, J., Hoffman, G., Wittig, C. 1988. *J. Chem. Phys.* 88: 2841–43
50. Wittig, C., Engel, Y. M., Levine, R. D. 1988. *Chem. Phys. Lett.* 153: 411–16
51. Shin, S. K., Wittig, C., Goddard, W. A. 1991. *J. Phys. Chem.* 95: 8048–53
52. Kudla, K., Schatz, G. C. 1991. *J. Phys. Chem.* 95: 8267–73
53. Sharpe, S. W., Zeng, Y. P., Wittig, C., Beaudet, R. A. 1990. *J. Chem. Phys.* 92: 943–57
54. Shin, S. K., Chen, Y., Oh, D., Wittig, C. 1990. *Philos. Trans. R. Soc. London Ser. A* 332: 361–74
55. Ohoyama, H., Takayanagi, M., Nishiya, T., Hanazaki, I. 1989. *Chem. Phys. Lett.* 162: 1–6
56. Hoffman, G., Oh, D., Iams, I., Wittig, C. 1989. *Chem. Phys. Lett.* 155: 356–62
57. Hausler, D., Rice, J., Wittig, C. 1987. *J. Phys. Chem.* 91: 5413–15
58a. Honma, K., Kajimoto, O. 1985. *Chem. Phys. Lett.* 117: 123–26
58b. Honma, K., Fujimura, Y., Kajimoto, O., Inoue, G. 1988. *J. Chem. Phys.* 88: 4739–47
59a. Schatz, G. C., Fitzcharles, M. S., Harding, L. B. 1987. *Faraday Discuss. Chem. Soc.* 84: 359–69
59b. Kudla, K., Schatz, G. C., Wagner, A. F. 1991. *J. Chem. Phys.* 95: 1635–47
59c. Aoyagi, M., Kato, S. 1988. *J. Chem. Phys.* 88: 6409–18
60. Gruebele, M., Sims, I. R., Potter, E. D., Zewail, A. H. 1991. *J. Chem. Phys.* 95: 7763–66
61. Metz, R. B., Bradforth, S. E., Neumark, D. M. 1991. *Adv. Chem. Phys.* 91: 1–61
62. Weaver, A., Metz, R. B., Bradforth, S. E., Neumark, D. M. 1988. *J. Phys. Chem.* 92: 5558–60
63. Waller, I. M., Kitsopoulos, T. N., Neumark, D. M. 1990. *J. Phys. Chem.* 94: 2240–42
64a. Metz, R. B., Kitsopoulos, T., Weaver, A., Neumark, D. M. 1988. *J. Chem. Phys.* 88: 1463–65
64b. Metz, R. B., Weaver, A., Bradforth, S. E., Kitsopoulos, T. N., Neumark, D. M. 1990. *J. Phys. Chem.* 94: 1377–88
65. Bradforth, S. E., Weaver, A., Arnold, D. W., Metz, R. B., Neumark, D. M. 1990. *J. Chem. Phys.* 92: 7205–22
66. Bradforth, S. E., Arnold, D. W., Metz, R. B., Weaver, A., Neumark, D. M. 1991. *J. Phys. Chem.* 95: 8066–78
67a. Weaver, A., Metz, R. B., Bradforth, S. E., Neumark, D. M. 1990. *J. Chem. Phys.* 93: 5352–53
67b. Zhang, J. Z. H., Miller, W. H., Weaver, A., Neumark, D. M. 1991. *Chem. Phys. Lett.* 182: 283–89
67c. Weaver, A., Neumark, D. M. 1991. *Faraday Discuss. Chem. Soc.* 91: 5–16
68. Manz, J., Meyer, R., Schor, H. H. R. 1984. *J. Chem. Phys.* 80: 1562–68
69. Schatz, G. C. 1989. *J. Chem. Phys.* 90: 3582–89; Schatz, G. C. 1989. *J. Chem. Phys.* 90: 4847–54; Schatz, G. C. 1989. *Is. J. Chem.* 29: 361–67; Schatz, G. C. 1990. *J. Chem. Soc. Faraday Trans.* 86: 1729–35; Schatz, G. C. 1990. *J. Phys. Chem.* 94: 6157–64
70a. Bowman, J. M., Gazdy, B. 1989. *J. Phys. Chem.* 5129–35; Gazdy, B., Bowman, J. M. 1989. *J. Chem. Phys.* 91: 4615–24
70b. Bowman, J. M., Gazdy, B., Sun, Q. 1990. *J. Chem. Soc. Faraday Trans.* 86: 1737–40
71. Zhang, J. Z. H., Miller, W. H. 1990. *J. Chem. Phys.* 92: 1811–18
72. Yamashita, K., Morokuma, K. 1990. *J. Chem. Phys.* 93: 3716–17
73a. Hahn, O., Gomez-Llorente, J. M., Taylor, H. S. 1991. *J. Chem. Phys.* 94: 2608–13
73b. Hahn, O., Taylor, H. S. 1992. *J. Chem. Phys.* 96: 5915–23
74. Kubach, C., Nguyen Vien, G., Richard-Viard, M. 1991. *J. Chem. Phys.* 94: 1929–38
75. Metz, R. B., Neumark, D. M. 1992. *J. Chem. Phys.* In press
76. Grayce, B. B., Skodje, R. T. 1991. *J. Chem. Phys.* 95: 7249–62
77. Ashford, M. N. R., Baggott, J. E., eds. 1987. *Molecular Photodissociation Dy-*

namics (*Advances in Gas Phase Photochemistry and Kinetics*). London: R. Soc. Chem. 243 pp.
78a. Imre, D. G., Kinsey, J. L., Field, R. W., Katayama, D. H. 1982. *J. Phys. Chem.* 86: 2564–66
78b. Imre, D. G., Kinsey, J. L., Sinha, A., Krenos, J. 1984. *J. Phys. Chem.* 88: 3956–64
79. Staemmler, V., Palma, A. 1985. *Chem. Phys.* 93: 63–69
80. Watanabe, K., Zelikoff, M. 1953. *J. Opt. Sci. Am.* 43: 753
81. Engel, V., Schinke, R., Staemmler, V. 1988. *J. Chem. Phys.* 88: 129–48
82a. Henriksen, N. E., Zhang, J., Imre, D. G. 1988. *J. Chem. Phys.* 89: 5607–13
82b. Zhang, J., Imre, D. G. 1989. *J. Chem. Phys.* 90: 1666–76
83. Pack, R. T. 1976. *J. Chem. Phys.* 65: 4765–70
84. Heller, E. J. 1978. *J. Chem. Phys.* 68: 3891–96
85. Kulander, K. C., Light, J. C. 1980. *J. Chem. Phys.* 73: 4337–46
86. Sension, R. J., Brudzynski, R. J., Hudson, B. S., Zhang, J., Imre, D. G. 1990. *Chem. Phys.* 141: 393–400
87a. Andresen, P., Ondrey, G. S., Titze, B., Rothe, E. W. 1984. *J. Chem. Phys.* 80: 2548–69
87b. Andresen, P., Beushausen, V., Hausler, D., Lulf, H. W. 1985. *J. Chem. Phys.* 83: 1429–30
88. Zhang, J. Z., Abramson, E. H., Imre, D. G. 1991. *J. Chem. Phys.* 95: 6536–43
89a. Thompson, S. D., Caroll, D. G., Watson, F., O'Donnell, M., McGlynn, S. P. 1966. *J. Chem. Phys.* 45: 1367–79
89b. Lee, L. C., Wang, X., Suto, M. 1987. *J. Chem. Phys.* 86: 4353–61
90. Klcinermanns, K., Linnebach, E., Suntz, R. 1987. *J. Phys. Chem.* 91: 5543–45
91. Person, M. D., Lao, K. Q., Eckholm, B. J., Butler, L. J. 1989. *J. Chem. Phys.* 91: 812–20
92. Brudzynski, R. J., Sension, R. J., Hudson, B. J. 1990. *Chem. Phys. Lett.* 165: 487–93
93a. Shih, S., Peyerimhoff, S. D., Beunker, R. J. 1976. *Chem. Phys.* 17: 391–402
93b. Guest, M. F., Rodwell, W. R. 1976. *Mol. Phys.* 32: 1075–89
93c. Heumann, B., Duren, R., Schinke, R. 1991. *Chem. Phys. Lett.* 180: 583–88
94. Dixon, R. N., Marston, C. C., Balint-Kurti, G. G. 1990. *J. Chem. Phys.* 93: 6520–34
95. Schinke, R., Weide, K., Heumann, B., Engel, V. 1991. *Faraday Discuss. Chem. Soc.* 91: 31–46
96. Nourbakhsh, S., Norwood, K., Yin, H.-M., Liao, C.-L., Ng, C. Y. 1991. *J. Chem. Phys.* 95: 946–54
97. Keller, J. S., Kash, P. W., Jensen, E., Butler, L. J. 1992. *J. Chem. Phys.* 96: 4324–29
98. Mouflih, B., Larrieu, C., Chaillet, M. 1988. *Chem. Phys.* 119: 221–32
99. Rose, T. S., Rosker, M. J., Zewail, A. H. 1988. *J. Chem. Phys.* 88: 6672–73; Rose, T. S., Rosker, M. J., Zewail, A. H. 1989. *J. Chem. Phys.* 91: 7415–36
100. Dantus, M., Rosker, M. J., Zewail, A. H. 1987. *J. Chem. Phys.* 87: 2395–97; Dantus, M., Rosker, M. J., Zewail, A. H. 1988. *J. Chem. Phys.* 89: 6128–40
101a. Bowman, R. M., Dantus, M., Zewail, A. H. 1989. *Chem. Phys. Lett.* 156: 131–37
101b. Dantus, M., Bowman, R. M., Gruebele, M., Zewail, A. H. 1989. *J. Chem. Phys.* 91: 7437–50
102. Gruebele, M., Roberts, G., Zewail, A. H. 1990. *Philos. Trans. R. Soc. London Ser. A* 332: 223–43

Annual Review of Physical Chemistry
Volume 43, 1992

CONTENTS

(*continued*)